PCCP

Accepted Manuscript

This article can be cited before page numbers have been issued, to do this please use: O. A. Pinto, B. A. Lopez de Mishima, E. P. M. Leiva and O. A. Oviedo, *Phys. Chem. Chem. Phys.*, 2016, DOI: 10.1039/C6CP05718G.

View Article Online
DOI: 10.1039/C6CP05718G

Simulation of the Selective Thermodynamic Deposition in Nanoholes

O. A. Pinto[1], B. A. López de Mishima[1], E. P. M. Leiva[2], and O. A. Oviedo[2,*]

1) Instituto de Bionanotecnología (INBIONATEC-CONICET), Universidad Nacional de Santiago de Estero, RN 9 Km 1125 Villa el Zanjón, Santiago del Estero, G4206XCP, Argentina.
2) Instituto de Investigaciones en Fisico-química de Córdoba (INFIQC-CONICET), Departamento de Química Teórica y Computacional, Facultad de Ciencias Químicas, Universidad Nacional de Córdoba, Córdoba, Argentina. X5000HUA.

*Corresponding author: o.a.oviedo@unc.edu.ar

Abstract

The deposition of particles in nanoholes is analyzed, taking into account the curvature of their inner walls. Different lattice-gas models of the nanoholes are considered. These include parallelepiped geometries, as well as holes shaped taking away from the surface pieces with polyhedral form. Several deposition stages are identified as a function of the degree of curvature of the inner walls of the nanoholes. The Monte Carlo technique in the Grand Canonical Ensemble is used to calculate isotherms, isosteric heats, energies per site and other thermodynamic properties. The study is based on different magnitudes for the interaction energies between the particles being deposited and those surrounding the nanohole.

1. Introduction

In the last few years, new experimental techniques have allowed to build new structures at the nanoscale, with amazing properties. It is a known fact that the structure (the atomic arrangement) is critical to define the thermodynamics properties of these nanostructures. In a first approximation, we can associate the difference of the thermodynamic properties of nanostructure with respect to macroscopic state (bulk), as a result of the deficiency in coordination which are subject some atoms. A nanostructure is small enough such that the amount of atoms with different coordination that the bulk are comparable to the latter. Therefore, it is necessary to consider a distribution of the coordination, instead of the average coordination. This distribution clearly depends on the size and shape of that nanostructure, and is one of the reasons why its thermodynamic properties depend on these parameters. As a result, traditional thermodynamics functions must be analyzed in a different way with respect to that used for bulky systems. It was originally done by T. Hill [1,2] in the 1960s, describing the thermodynamic properties of tiny objects, made of a few atoms. This word led to a new area of study, denominated

View Article Online
DOI: 10.1039/C6CP05718G

nanothermodynamics. One outcome of Hill´s theory is that the thermodynamics properties of nanomaterials may vary with the size of it, such as melting of small particles [3,4], chemical reactivity [5], diffusivity [6], sintering [7], and electrodeposition [8,9].

We can classify the nanostructures in two categories: those with positive or negative curvatures. The first include for example the nanoparticles (NPs), nanotubes, and/or supported clusters while the second include for example the nanocavities, pinholes, and nanoholes (NHs). Nanostructures with positive curvature are usually defined as polyhedra usually formed by facets type {111} and {100} connected by border of low coordination. Nanostructures with negative curvature are defined generally with the same facet types, but connected by border of high coordination. This subtle and delicate structural difference means that they can have the inverse physical and chemical properties [10]. For example, the adsorption energy inside of the a negative curvature nanosystems is favored, while that on a positive curvature nanosystem is weakened [11,12,13]. Recently a special type of nanosystems with negative curvature, called NPs with open surfaces or faceted high rates (H-NPs) have proved are important in technological applications such as chemical catalysis [14,15,16,17,18,19]. The H-NPs are nanosized crystals formed by facets with at least one Miller index {hkl} greater than unity. The surfaces of the H-NPs are characterized by a high density of steps with low coordination, which give a great surface energy. This allows them to exhibit a marked increase in the electrocatalytic activity, such as in the electrooxidation of methanol, ethanol and/or formic acid [20,21]. The latter has led to the increasing development of this synthetic strategies, handling and methods of integrating these devices at the nanoscale in order to obtain products with novel physicochemical properties that are difficult to obtain in bulk materials or positive curvature nanostructures.

Nanostructuring at the electrochemical interphase has been applied successfully by scanning tunneling microscope (STM), where the potentials of the tip and of the substrate can be controlled separately by means of a bipotentiostat, allowing great flexibility to study surfaces under a variety of polarization conditions. In the case of the electrochemical use of STM, a number of applications have appeared that allow study and generate nanostructures. For example, NHs have been produced by crash a tip of the a STM on a metallic surface [22,23,24,25,26,27,28]. This techniques has also been used to create NHs on the non metallic surface such as graphite, and then filled with Ag stemming from the STM tip [29]. In other type of approach, NHs were created without contact, it is by the application of short negative voltage pulses to a STM tip and then filled with Cu clusters [30,31,32]. These defects play an important role because it can act as nucleation centers and allow further growth of other metal nanostructures. If the potential applied to the substrate is controlled carefully, it is possible to confine the deposition from the solution to the volume inside the NH, where the nucleation sites are provided by the edges or steps inside the NHs. Electrodecoration with other metals were also analyzed such as Bi and Ag, which were deposited on Au-NHs, using the same technique aforementioned [33,34,35].

Thermodynamic and structural properties of the NHs, have been previously studied by Off-lattice Monte Carlo simulations using Embedded Atom Method (EAM) potentials [23,24,25,26]. In the Cu deposition on Au-NHs case, sites linked with four substrate atoms in the inner wall of the NH were

View Article Online
DOI: 10.1039/C6CP05718G

identified as the places where growth of Cu begins (an nucleation preferential). When the chemical potential of Cu was increased the NH was filled up to the surface level, then was detected the formation of a 3D-cluster on this surface. On the other hand, in Ag electrodeposition on Au-NH case the filling of the NH was described by a 2D layer-by-layer mechanism and no 3D-cluster formation. While NHs have been the same in both simulations, it can be inferred that the interaction between species is the cause of this peculiar behavior.

Recently, we have analyzed systematically nanoeffects in several thermodynamics properties on positive curvature, such as NPs [36,37]. There, we employed Grand Canonical Monte Carlo (GCMC) simulations and/or analytic approaches under lattice gas approach. Size of the nanostructure was used that a key parameter that allowed the understanding of adsorption properties in the nanoscale.

Particularly, the surface adsorption on several nanoparticle geometries with repulsive interaction has previously been tackled for us, in Reference **[38]**. There, we considered interactions between lateral nearest neighbors and with the substrate itself. In that case the coordination number varied from zero to nine. These interactions were responsible for the formation of several ordered structures on the surface of the nanoparticles, which exhibit a ***positive*** curvature. In the present work, we extend the analysis to the deposition on nanoholes, which present a ***negative*** curvature. Although a similar simulation scheme is followed, two important differences can be drawn:

- In the case of surfaces with negative curvatures like the present ones, the coordination number of the deposited atoms is increased(up to twelve) with respect to the case of adsorption on planar surfaces. The opposite is the case for atom adsorption on nanoparticles, where the coordination number is decreased.
- The deposition process can take place on the surface and on the entire volume defining the nanostructure.

So, the present work is a continuation of these studies. The main objective is the systematic thermodynamic characterization of deposition in NHs with different size and geometries, within a lattice gas scheme. Here, the curvature in the inner walls of the NH is taken as a key parameter of the process. The GCMC method, which involves the creation and annihilation of particles in equilibrium with a reservoir of particles at a fixed chemical potential is used with this purpose. In principle, the main aim is the emulation of electrochemical deposition, but the conclusions may be valid for related systems with control of the chemical potential of adsorbing particles as well.

2. Models and basic definitions

As above stated, particle deposition will be simulated by assuming that the chemical potential of the deposited particles is controlled by equilibration with the chemical potential of particles in an infinite reservoir. Three lattice gas models will be considered. Model A, represents a tridimensional solid, where

View Article Online
DOI: 10.1039/C6CP05718G

the NH has a parallelepiped geometry. The solid is formed by four planes of atoms separated by a distance corresponding to the separation between lattice planes of the single crystal surface exposed by the metal. In three of them a square nanohole is created where the inner walls present no curvature. On the upper surface, atoms can be deposited and form a monolayer. The surface geometry corresponds to the (100). A NH of this type is illustrated in Figure 1a. The red spheres correspond to the atoms of the solid and the empty sites are represented as white spheres. The total number of sites on the external surface is $(L+2l)^2$, where L is the number of missing atoms in the border of the NH, and l is the number of atoms in one border of solid. The depth is quantified by the n-index and corresponds to the total number of planes involved in the NH. Because all planes have the same L, each plane of the NH has L^2 missing atoms. Then, the volume of the NH, expressed in atomic units, is $V_{NH-A} = nL^2$. In Model A, we consider $n=3$, $L=30$, and $l=5$.

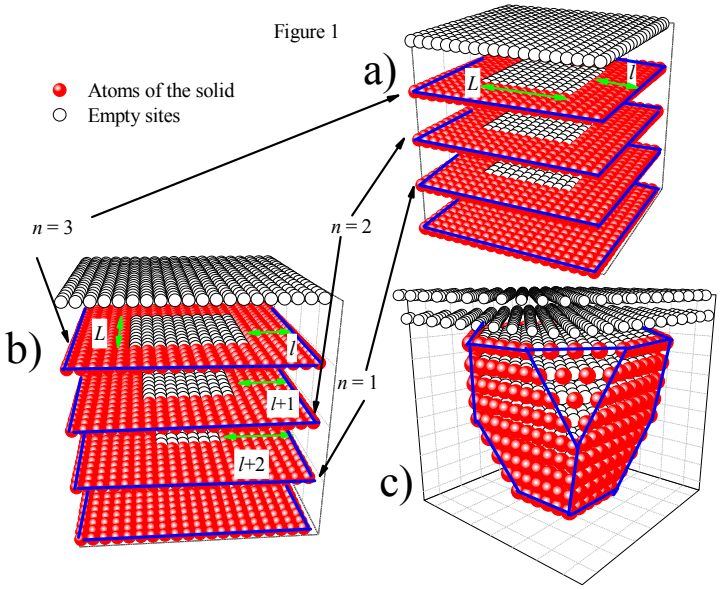

Figure 1: Snapshot of the models. The insets a), b) and c) correspond to models A, B and C respectively. The blue lines are guide eyes.

The second model, called Model B, includes curvature effect in the inner walls. This curvature effect is modeled considering a one-atom step inwards per each plane in the NH. Thus, the plane $n=3$ (considering $n=1$ to be the bottom layer) has L^2 empty sites. The plane with $n=2$ has $(L-2)^2$ sites and finally for $n=1$, the number of empty sites are $(L-4)^2$. The NH volume for this Model is

View Article Online
DOI: 10.1039/C6CP05718G

$V_{NH-B} = L^2 + (L-2)^2 + (L-4)^2$. **Figure 1b** shows the geometry of the system. The blue lines are a guide to the eyes to grasp the geometry of the models.

Finally, the third model, called Model C considers a more realistic type of curvature. The NH is formed in this case by detaching atoms from the solid which corresponding to the half of a pristine truncated octahedron (TO) NP, with a facet type {100} directed towards the surface. Thus, the shape of the cluster that the adsorbate will define upon completion of the NH will be TO. Therefore, NHs are formed by facets type {111} and {100} connected by border of high coordination. The sites at the center of the empty NH have twelve nearest neighbors (NN), but this number decreases as we move towards the border of the NH. In this model we have extended the net for adsorption until two layers above the surface of the solid. **Figure 1c**, shows the geometry of this Model.

We turn now to define the energetic parameters for these models. We consider the solid substrate to be constituted by particles of type α. Particles of type β (adsorbate) can be adsorbed on the inside of NH and on the surface of the solid. From thermodynamic point of view, the deposition conditions are characterized by the chemical potential μ at temperature T. Only nearest-neighbor interactions are considered. The adsorbates can thus "feel" two kinds of interactions: an heteroatomic and/or an homoatomic, that we assign ε and w respectively. The Hamiltonian can be written as:

$$H = \sum_{\langle (i,j,k),(i',j',k') \rangle} c_{i,j,k} c_{i',j',k'} \left[\left(\frac{c_{i',j',k'} - 1}{2} \right) w + \left(\frac{c_{i',j',k'} + 1}{2} \right) \varepsilon \right] \qquad (1)$$

The indices i, j and k correspond to space coordinates in the solid. $c_{i,j,k}$ is zero if site (i, j, k) is empty or 1 if occupied by a β particle. The sum runs over adsorption sites only and multiple occupations are forbidden. The adsorption-desorption process is simulated by a standard importance sampling Monte Carlo method in the Grand Canonical Ensemble [39,40,41]. To satisfy the principle of detailed balance, we used the Metropolis algorithm [42].A Monte Carlo Step (MCS) corresponds to M attempts to change the state of the system. Before sampling the quantities of interest, thermodynamic equilibrium was established, this condition was attained discarding the first 5×10^6 MCSs. Then, the next 2×10^6 MCSs were used to compute averages and the parameters of interest were obtained by simple averages.

For the two first models considered, partial coverages were defined according to:

$$\theta_n(\mu,T) = \frac{\langle N_n \rangle}{L^2} \qquad \text{with } n\text{=1, 2 and 3} \qquad \text{Model A} \qquad (2a)$$

View Article Online
DOI: 10.1039/C6CP05718G

$$\theta_1(\mu,T)=\frac{\langle N_1\rangle}{L^2},\quad \theta_2(\mu,T)=\frac{\langle N_2\rangle}{(L-2)^2},\quad \theta_3(\mu,T)=\frac{\langle N_3\rangle}{(L-4)^2} \qquad \text{Model B} \qquad (2b)$$

where the indices "*n*" indicate each lattice plane considered in the NH models (see **Figure 1**). N_n is the number of particles deposited in each *n*-plane, and the brackets denote averages taken along the simulation. The full coverage was computed as:

$$\theta(\mu,T)=\sum_i \theta_i(\mu,T) \qquad (3a)$$

or equivalently

$$\theta(\mu,T)=\frac{1}{V_{NH}}\sum_i \langle c_i\rangle \qquad (3b)$$

As the total coverage is normalized to volume of the NH, $\theta=1$ means a full NH. Since the volume is expressed in atomic units, the energy per particle in the NH is calculated as:

$$u(\theta)=\frac{\langle H\rangle}{V_{NH}} \qquad (4)$$

The differential heat of adsorption is in turn:

$$q_d(\theta)=-\frac{\partial u}{\partial \theta}=\frac{\langle NH\rangle-\langle H\rangle\langle N\rangle}{\langle N^2\rangle-\langle N\rangle^2} \qquad (5)$$

View Article Online
DOI: 10.1039/C6CP05718G

For Model C, Eqns (3b), (4) and (5) can be applied, taking into account that V_{NH} are sites inside of the NH.

In this statistical assembly it is possible to obtain the quasi-equilibrium voltammograms (current versus electrode potential plots) associated with the adsorption isotherms. The current may be obtained from the fluctuations in the number of particles on the surface of the NH, which also corresponds to the compressibility of the adlayer:

$$i \propto \frac{d\langle N\rangle}{d\mu} = \frac{\langle N_B^2\rangle - \langle N_B\rangle^2}{kT} \qquad (6)$$

The electrode potential is linearly related to the dimensionless quantity $\beta\mu$, so that a plot of the quantity on the RHS of Eqn (6) as a function of $\beta\mu$ resembles the voltammetric curve. For a detailed explanation, the reader is referred to [**Error! Bookmark not defined.**].

3. Results and discussion

In this section we describe the thermodynamic behavior of the three models proposed above.

3.1 Model A

As stated above, this model represents an idealized NH with parallelepiped geometry. The energies will be expressed in k_BT units, where k_B is the Boltzmann constant $\left(8,6173324\times10^{-5}\,\mathrm{eV\,K^{-1}}\right)$ and $k_BT = 0.0258$ eV. We have considered for adsorbate-substrate and adsorbate-adsorbate interaction as: $w/k_BT = -1.0$ and $\varepsilon/k_BT < 0$, respectively. These energetic parameters are usually used for describe attractive interactions that are typically involved in metallic depositions. The values considered were $\varepsilon/kT = -0.5,\ -0.75,\ -1.0,\ -2.0,\ -5.0$ and -7.0, corresponding to describe a more favorable (negative) bond between adsorbates. With these negative interactions, the adsorbate tries to adsorb in sites with a maximum coordination. For dimensioning the energy values used , we can mention that per bond energy of the Ag and Pt atoms bulk in k_BT units are -18.0 and -37.0, respectively at room temperature. **Figure 2** shows the corresponding adsorption isotherms,

View Article Online
DOI: 10.1039/C6CP05718G

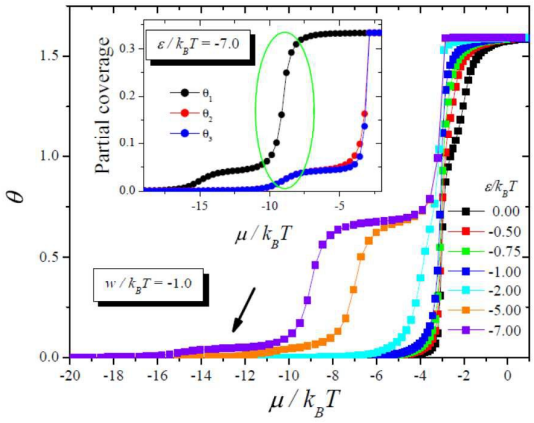

Figure 2: Adsorption isotherms for Model A. The inset shows the partial coverages.

The coverage inside of the NH can be calculated from $\theta_{\max}(L,l)=1+(L+2l)^2/3L^2$, so that $\theta_{\max}(L=30,\ l=5)=43/27$. For $\varepsilon/kT<-5$, all isotherms saturate at the same value. In the case where $\varepsilon/kT=w/kT=-1.0$, the adsorbates have the same probability of sticking at the bottom of the NH as to adsorb on surface sites. We can consider the bottom of the NH as a simple heterogeneous substrate. For $\varepsilon/kT>w/kT$ we observe a progressive filling until the formation of the monolayer on surface of the solid. In the opposite case, when $\varepsilon/kT<w/kT$, we observe the occurrence of two broad plateaus previous to saturation. The first one (marked with an arrow in **Figure 2**) corresponds to the filling of the vertices and edges sites of the bottom plane. The inset shows the partial coverage of each plane for c. In this inset, the isotherm for the bottom plane (θ_1), shows a plateau at $\theta_1\approx 0.05$ corresponding to the first plateau in the total isotherm. It is interesting to observe a simultaneous increase in θ_2 and θ_3 practically at the same chemical potential. This corresponds to the filling of the vertices sites at each plane. A green ellipse is drawn to emphasize the mentioned phenomena in the inset of **Figure 2**. The third plateau observed at saturation coverage θ_{sat-A}, corresponds to complete filling of the adsorption sites.

When the bottom plane is completely filled, $(\theta_1\approx 0.33)$ the others planes begin to fill until saturation, reaching $\theta_2=\theta_3\approx 0.04$. This means that the inner walls of the NH are decorated. The second plateau at $\theta\approx 0.67$ corresponds to the filling of the full inner walls plus the formation of a monolayer on the solid. At this point, all the surfaces exposed are completely decorated by adsorbate particles. Thus, the system minimizes its energy by maximizing the number of intra-particle pairs. After this, the NH is completed by a condensation mechanism, manifested by a prompt jump in the isotherms from the second plateau until θ_{sat-A}. This behavior is typical for attractive interactions [36,37]. To clarify the nature of this stage, **Figure 3** shows snapshots of that GCMC simulation. **Figure 3a** correspond to the first plateau of the case $\varepsilon/kT<-5.0$, where a "square ring" is observed at the bottom plane and the vertices of the other

View Article Online
DOI: 10.1039/C6CP05718G

planes are filled. The filling of the entire surface exposed is shown in **Figure 3b**, in correspondence with the second plateau occurring at the total isotherms.

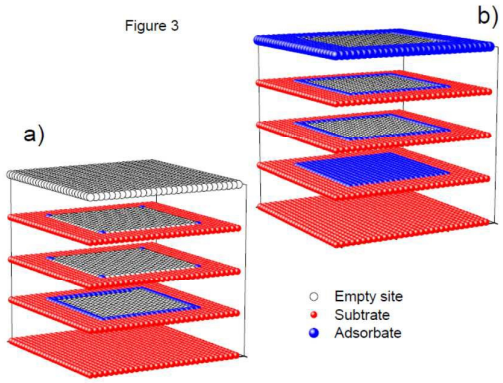

Figure 3: State of occupation of the systems for Model A: a) first plateau, b) second plateau given in **Figure 2**.

The energy per site as a function of the coverage degree is shown in **Figure 4a**. For the isotherms with a progressive filling (without steps), the energy presents a smooth curve. For the other case, the energy shows a change in the slope at the coverage where take place the plateaus in the isotherms. The inset shown a zoom indicate this slope change for the first plateau. A discontinuity is observed in correspondence with the condensation reported in isotherms. Another interesting thermodynamic parameter is the differential heat, because it can be measured in experimental setups. This parameter can be computed from fluctuations, see Eqn. (5). **Figure 4b** show steps can be identified at the coverages where the plateaus appear in the isotherm. The steps become more evident as the plateaus are wide. The black arrow indicates the first step for the case $\varepsilon / kT = -7.0$.

View Article Online
DOI: 10.1039/C6CP05718G

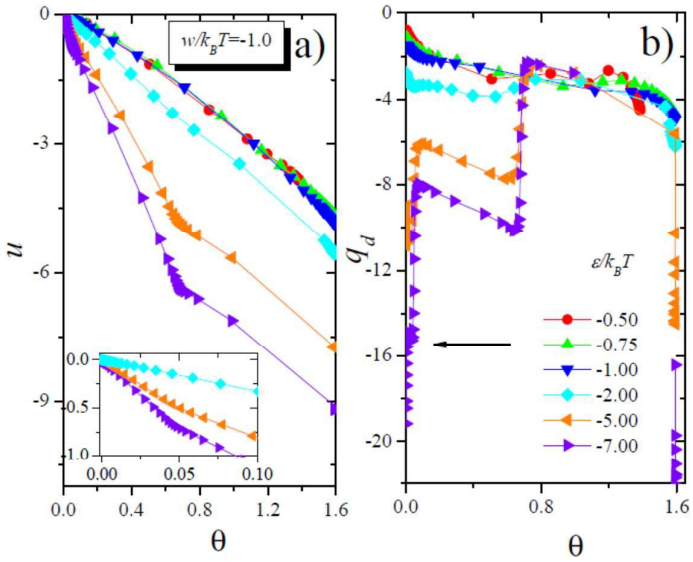

Figure 4: a) Energy per site as a function of the coverage degree. The zoom indicate this slope change for the first plateau. b)The differential heat as a function of the coverage degree; the black arrow indicates the first step for $\varepsilon / kT = -7.0$.

Now, we analyze the effect of NH size L. With this aim, we consider the isotherms obtained with $L = 2,\ 5,\ 10,\ 20$ and 30 (l=5 and n=3) for the case of $\varepsilon / kT = -5.0$,where the plateaus are visible. These isotherms are shown in **Figure 5**. All the plateaus described previously are observed at $L > 5$. It is found that the saturation of the adsorption isotherm depends on L. At $L < 10$ the first plateau becomes less evident.

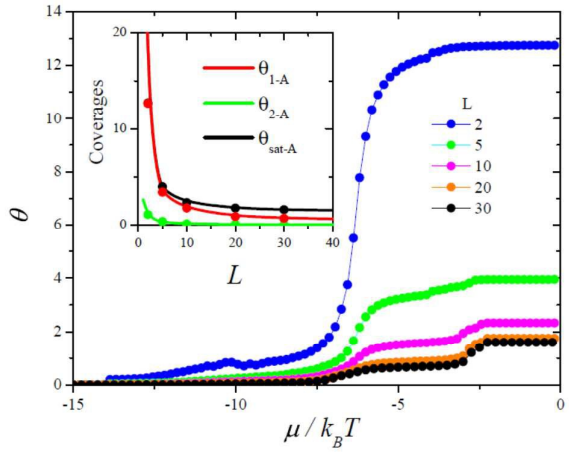

View Article Online
DOI: 10.1039/C6CP05718G

Figure 5: Adsorption isotherms for l=5, n=3 and $\varepsilon/kT=-5.0$ for several values of L, The lines in the inset are the recurrence relations of saturation coverages, given in Eqns. (7-9). The points were obtained from the simulations.

A question that we want to answer is whether the plateaus are observable for large values of L. For this purpose, we can write relations for first plateau θ_{1-A}, the second plateau θ_{2-A}, and the saturation coverage θ_{sat-A}, respectively as:

$$\theta_{1-A}(L)=\frac{4L+4}{V_{NH}}=\frac{4L+4}{3L^2} \qquad (7)$$

$$\theta_{2-A}(L)=\frac{N_{SNH}}{V_{NH}}+\frac{N_{surf}}{V_{NH}}=\frac{L^2+12L-12}{3L^2}+\frac{4lL+4l^2}{3L^2}\bigg|_{l=5}=\frac{L^2+32L+88}{3L^2} \qquad (8)$$

$$\theta_{sat-A}(L)=\frac{3L^2+(L+2l)^2}{V_{NH}}=\frac{3L^2+(L+2l)^2}{3L^2}\bigg|_{l=5}=\frac{4L^2+20L+100}{3L^2} \qquad (9)$$

where N_{SNH} is the number of sites on the inner walls of the NH and N_{surf} is the number of sites on the external surface. These expressions are plotted as a function of L in the inset of **Figure 5**, while the dots are obtained from GCMC simulations. We observe a good agreement. If $L\to\infty$, the walls are very far from each other and we get $\theta_{sat-A}(L)\to 4/3$, $\theta_{1-A}(L)\to 0$ and $\theta_{2-A}(L)\to 1/3$. The first plateau disappears as expected while the others reach a constant value. For the second plateau, in this approach, the area of the bottom plane is imposed on the other areas involved.

3.2 Model B

Now we describe the thermodynamic behavior of Model B, with the idea of analyzing the effect of small curvatures in the inner walls of the Model A. **Figure 6** shows the adsorption isotherms for several values of reduced energies, ε/kT, at $L=30$. When the energies ε/kT change to more negative

View Article Online
DOI: 10.1039/C6CP05718G

values, two broad plateaus are observed. The inset shows partial coverages, for $\varepsilon / kT = -10.0$. At low chemical potentials, the three variables, θ_1, θ_2 and θ_3, increase simultaneously; this is marked with an ellipse in the inset of **Figure 6**, and means that the inner walls are filled at once, remaining the bottom of the cavity uncovered. This corresponds to the first plateau in the total isotherm at $\theta \approx 0.13$. The subsequent partial saturation of θ_1 corresponds to the filling of the bottom plane. The second plateau on the total isotherm corresponds to the filling of the surface sites, including the monolayer. At this point, all exposed surfaces are decorated with β-particles. After this, the NH is filled through a condensation. Snapshots are shown in the **Figure 7** that correspond to a) the first plateau and b) the second plateau.

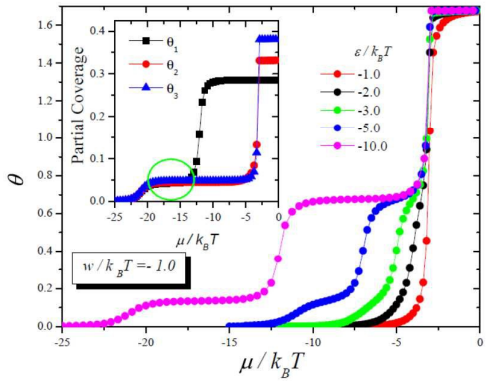

Figure 6: Adsorption isotherms for Model B at $L = 30$. The inset shows the partial coverages.

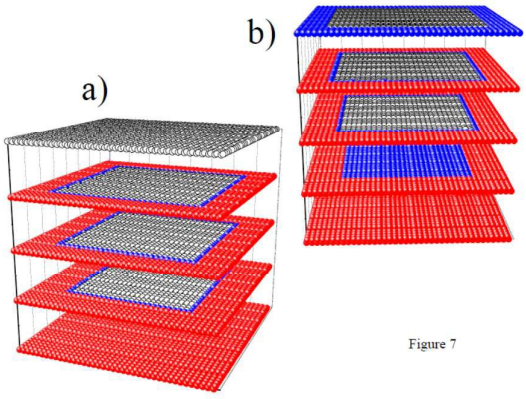

Figure 7: Snapshots for Model B; (a) for the first plateau and b) for the second given in **Figure 6**.

View Article Online
DOI: 10.1039/C6CP05718G

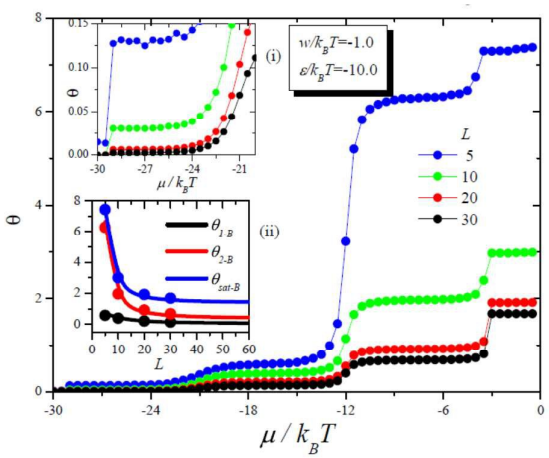

Figure 8: Adsorptions isotherms for $\varepsilon / kT = -10.0$ and different values of L for Model B. The inset i) shows a zoom of the first plateau. The inset ii) shows saturation coverages for the recurrence relations (lines) given in Eqns. (10-12) and GCMC simulations (points).

Figure 8 shows the isotherms for $\varepsilon / kT = -10.0$ and different values of L. The behavior of the isotherms is similar that of Model A, but a third plateau can be observed at very low coverages. This plateau becomes visible for strong negative values of the intra-particle energy, and small *Ls*. It is important to mention than $L = 5$ is the minimum size that conserves the characteristic of the NH for the present model. This first plateau corresponds to adsorption on sites where number of intra-particle links are maximized. These are the corners of each plane. At these sites each adsorbate is linked with three particles of the solid. Inset (*i*) corresponds to a zoom on this first plateau. As in the previous case, a equation can be obtained relating L with θ_{1-B}, θ_{2-B} and θ_{sat-B}, which correspond to the first plateau, the second plateau and the full coverage respectively:

$$\theta_{1-B}(L) = \frac{12L - 36}{3L^2 - 12L + 20} \qquad (10)$$

$$\theta_{2-B}(L) = \frac{L^2 + 10L + 158}{3L^2 - 12L + 20} \qquad (11)$$

$$\theta_{sat-B}(L) = \frac{10L + L^2 + 150}{3L^2 - 12L + 20} + 1 \qquad (12)$$

View Article Online
DOI: 10.1039/C6CP05718G

Inset (*ii*) shows these quantities as a function of *L*. For the thermodynamic limit ($L \to \infty$), we get $\theta_{sat-B}(L) \to 4/3$, $\theta_{1-B}(L) \to 0$ and $\theta_{2-B}(L) \to 1/3$. The points in the inset are obtained from GCMC simulations, and as found above for Model A. Here, there is also a good correspondence with the analytical relations. The features of the energy per site and the differential heat (not show) are in complete agreement with behavior of the isotherms. The energy presents a change of slope and the differential heat a step associated with each deposition regime. In similar way to that of Model A, the first plateau disappear in the large *L* limit because the walls are very far from each other.

3.3 Model C

To take into account explicitly the effect of curvature in a realistic systems, a NH was build using {111} and {100} facet, corresponding to the most frequent crystal planes in the experiments. In Section 2 we explained how were building this structures. Inner walls of the NH are formed by two different kind of facets, *i.e.* {100} and {111}. In addition two layers are considered on the (100) surface of the solid. We considered an size of full layer containing 800 sites and the same parameter of Model A, $w/kT = -1.0$.

Figure 9 shows the isotherms from several values of ε/kT for $V_{NH} = 331$ (in atomic units), this volume correspond to the half of TO. For $\varepsilon/kT = -1.0$, the sequence of deposition can by resume as follows: NH is filled in the first place, second the monolayer and finally the bilayer are formed. As we know at these energies take place a no preference sites, the most coordinated sites are the first to be occupied; this corresponds with the sites in the inner of the NH. An interesting point to consider, is on how large must be the temperature of the system so that the energetic landscape is blurred by thermal effects. This depends in a complex way on ε, w and on the topology of the heterogeneous surface. The present simulations show that the step associated with the structure illustrated in snapshot 10c becomes evident for weakly attractive systems, where $\varepsilon/kT \leq -3$, involving energies interaction of the order of $\varepsilon \approx -0.08$ eV. On the other hand, the step related to the structure shown in snapshot 10b becomes evident for interactions where $\varepsilon/kT \leq -5$.

View Article Online
DOI: 10.1039/C6CP05718G

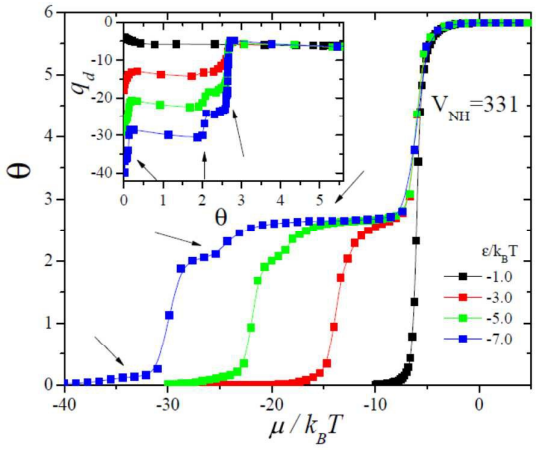

Figure 9: Adsorption isotherms for Model C. The arrow marks the plateaus. The inset shows the differential heat q_d. Steps are indicated with arrows.

Figure 10

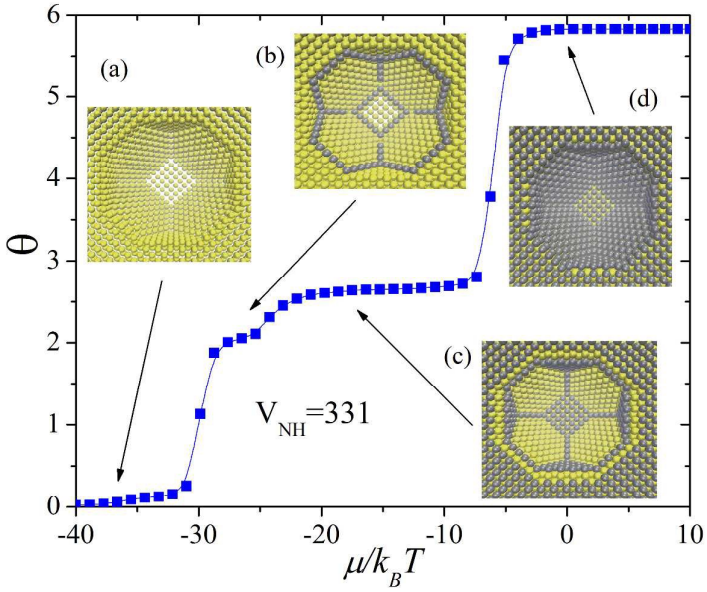

Figure 10: Adsorption isotherm for Model C at $\varepsilon / kT < -7.0$. The inset shows snapshots of top view for Model C. The yellow spheres represent the substrate and the greys are adsorbate.

However, when $\varepsilon / kT < -1.0$, several plateaus are observed. All of them are pointed by black arrows at the isotherm of $\varepsilon / kT = -7.0$. The insets in Figure 10 shows, the snapshot associated to each plateau. The inset (a) shows the empty substrate. The second plateau corresponds to the occupancy of the borders and vertices sites (inset **b**). The border sites are those that link each facets. The third plateau correspond to the filled of the {100} facet inside of the NH and on the (100) surface of solid (inset **c**). The

View Article Online
DOI: 10.1039/C6CP05718G

fourth plateau corresponds to the occupation of the {111} facets inside the NH (inset **d**). At this point the entire surface is decorated by the adsorbate. It is interesting to note that snapshots 10b and 10c exhibit a complex composition, involving different coordinations of the adsorbate with the substrate. These structures could not have been inferred on simple coordination considerations. Finally NH is filled and the second layer is formed (not shown) by a condensed mechanism. Similarly to the previous observations, the energy per site presents a change of slope at the coverages where the plateaus are observed. The differential heat q_d is shown in the inset of **Figure 9**. Steps are observed corresponding to each plateau reported in the isotherms and are marked by arrows. The intensity of the steps depends on the values of w/kT .

Figure 11 shows the dependence of the isotherms with V_{NH} for $\varepsilon/kT=-5.0$ and $w/kT=-1.0$. When the size of the NH is decreased, all the previous plateaus are observed but they are shifted toward high values. The inset shows the differential heat, where the mentioned shift is observed too.

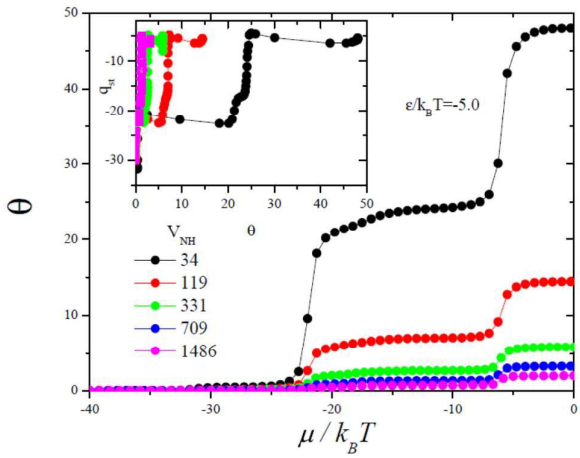

Figure 11: Adsorption isotherms with the different quantity of inner sites in Model C, for several values of V_{NH}. $\varepsilon/kT=-5.0$ and $w/kT=-1.0$. The inset shows the differential heat as a function of θ .

In order to analyze the experimental implications that arise from the present modeling for electrochemical deposition, we consider in this section the effect of the increase in the curvature of a NH. With this purpose, the NH was characterized through three variables: M, L and a . The first parameter indicates the number of lattice planes defining the depth of the NH. The second parameter, L, indicates the size (in atomic units) of the square base (bottom) of the NH. The third parameter, a , indicates the width (in atomic units) of the terraces that constitute the walls of the NP (considered all of the same width). The inset in **Figure 12a** schematically forms such characterization. **Figure 12a** shows the adsorption

View Article Online
DOI: 10.1039/C6CP05718G

isotherms for a NH which is 5 lattice planes deep (M=5), with different terrace sizes, a =2, 4, 6, 8 and 10, using in all cases $\varepsilon / kT = -7.0$ and $w / kT = -1.0$. When a increases, the curvature of the NP decreases.

In agreement with the three models mentioned above, the present isotherms show 4 stages:

1) Filling of vertices, $(\mu / kT \approx -21.0)$.

2) Filling of the edges, this corresponds to the formation of "square rings" reported in model B, $(\mu / kT \approx -15.0)$.

3) Decoration of the steps between the facets, $(\mu / kT \approx -9.0)$.

4) Complete filling of the NH (bulk-like deposition) $(\mu / kT \approx -3.0)$.

Adsorption isotherms such as those shown in this paper can be obtained from electrochemical experiments, from the analysis of charge flow on a conductive surface, as a function on the deposition potential **[43]**. The i vs V curves (voltammograms), can be obtained taking the derivative of the coverage with respect to the potential. Alternatively, statistical mechanics also offers the possibility to compute the voltammograms from the theory of fluctuations. In fact, it possible to emulate i vs V curves through computer simulations by the analysis of the root mean square fluctuations $\left(\langle N^2 \rangle - \langle N \rangle^2\right)$ as a function of the normalized chemical potential $(\beta\mu)$. However, it is necessary to point out that quasi equilibrium conditions are required to compare experiment with Monte Carlo simulations **[38]**.

Figure 12b shows the fluctuations (which are proportional to the experimental voltammograms) for different negative curvatures of the NH. Independently of the size of the terraces, it is found that all current peaks occur at approximately the same potential. This indicates that the positions of these maxima only depend on the energetic parameters **[36,37,38]**, so that small changes in the curvature of NH only modifies the intensities in the voltammograms. Then, we can infer that an analysis of the relative contributions of these intensities can be used to infer the shape of the NH. This is not a simple task, since besides the analysis of different shapes of the NH, it is necessary to consider the variation of fluctuations with size (see inset **Figure 12b**). In the case of macroscopic systems, the fluctuation of the number of particles is negligible as compared with system size. However in the nano world this is not necessarily correct. These studies are in progress and will be subject of subsequent publications.

View Article Online
DOI: 10.1039/C6CP05718G

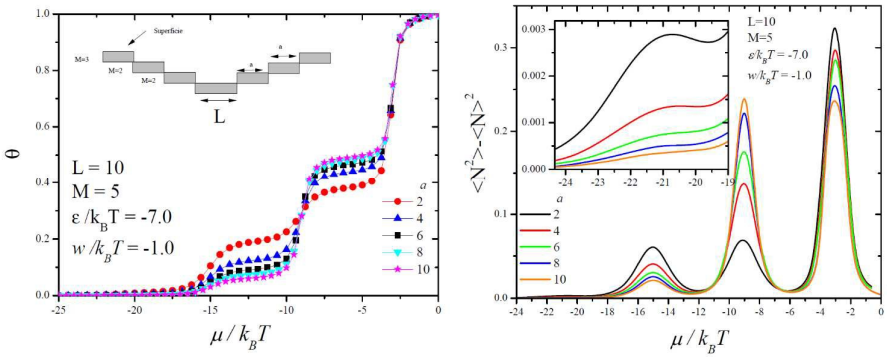

Figure 12: a) Adsorption isotherms for nanoholes with different negative curvatures, using $\varepsilon / kT = -7.0$ and $w / kT = -1.0$. The inset shows the model used to characterize a negative curvature. b) Mean square fluctuations as a function of the normalized chemical potential for a NH with different curvatures at 300 K. The inset corresponds to a zoom of the initial stage of deposition.

4. Conclusions

In this paper we have modeled the deposition on nanoholes (NH) with three different lattice gas models. Two kinds of energetic interactions were considered: interparticle ε, and intraparticle *w*. Model A emulates an idealized nanohole as a solid with vertical walls. The hole was only three atomics planes deep. Attractive interactions were assumed in all cases, which could be associated with the interaction arising between metal atoms. The analysis was done as a function of different values of w / kT . The isotherms show the occurrence of two plateaus, which are related to the different regimes of decoration in the NH. The surface of NH was considered as a heterogeneous substrate. The first plateau is associated with deposition on vertices and edges at the bottom plane. The second plateau is associated with the formation of the monolayer and the decoration of all the inner walls. The differential heat and the energy per site are in agreement with the results of the isotherms. When the size of the NH is changed, the isotherms present a different regimen of saturation, which can be recognized as a nanoeffect. Analytical equations allow to analyze the tendencies found for big size of NH. The first plateau disappears in this limit (border effects become negligible), and the second one reaches a constant value. In this limit, it is reasonable to think than at very large distances between the inner walls the system can be considered as a two dimensional substrate. Another important conclusion reached is that the formation of the monolayer occurs before the filling of the nanohole, which takes places at last.

Model B includes a curvature in the inner walls. In this case there are three stages of deposition; the first corresponds to adsorption on sites where the number of adsorbate-substrate links is maximum. These are vertices sites, and the nanoeffect only is visible at very low values of *L*. The second corresponds to the filling of inner walls only. Finally, the last plateau corresponds to the filling of the bottom plane and the monolayer.

View Article Online
DOI: 10.1039/C6CP05718G

In summary, both models, A and B, present intermediate states before the complete filling of the NH. The previous states depend on the distribution of lateral links in the models. The curvature allows the filling of the inner walls before the bottom, as it was the case of Model A. However, in the model B, there is not preference between facets or bottom. This general behavior does not depend on the quantity of inner planes considered, even if we consider a solid with geometry (111).

Model C, considers a more realistic NH with the internal geometry of an truncated octahedron. This presents a distribution of links that depends on the position in the NH. When the interparticle and intraparticle interactions are the same values, the NH is filled before the layers. But when $w/kT < \varepsilon/kT$, the situation is opposite. All the surfaces are decorated before the filled of the NH. This is an effect of the curvature and the kind of interactions analyzed.

The positions of the current peaks in the simulated voltammograms depend only on the energy parameters, so that small changes in the curvature modify the relative intensities of the peaks in the voltamograms. This can be used to infer, through an analysis of the relative contributions of current intensities, the size and shape of the nanocavity.

5. Acknowledgments

The authors acknowledge financial support from Universidad Nacional de Santiago del Estero, under project CICyT-UNSE 23 A173, CONICET PIP 11220110100992, SECyT Universidad Nacional de Córdoba, Program BID (PICT 2012-2324), and PME: 2006-01581 of Argentina. The numerical work were done using the Huauke parallel cluster (located in Instituto de Bionanotecnología (INBIONATEC-CONICET), Universidad Nacional de Santiago de Estero, Argentina.

6. References

[1] T. L. Hill. Thermodynamics of Small Systems (Parts I and II) (Dover Publications, New York, (1994).
[2] T. L. Hill, Nano Lett. 1 (2001) 273.
[3] F. Ercolessi, W. Andreoni and E. Tosatti. Phys. Rev. Let. 66 (1991) 7.
[4] J.P. Borel, Surf. Sci. 106 (1981) 1.
[5] C.N.R. Rao, G.U. Kulkarni, P.J. Thomas and P.P. Edwards. Chem. Euro. J 8, 28e35, (2002).
[6] S. Horch, H.T. Lorensen, S. Helveg, E. Laegsgaard ,I. StensgaardI, and K.W. Jacobsen, J. K. Nørskov and F. Besenbacher. Nature (London) 398 (1999)134e6.
[7] S. Mintova, N. H. Olson, V. Valtchev and T. Bein. Science 283, (1999) 958e60.
[8] O.A. Oviedo, E.P.M. Leiva and M.M. Mariscal. Phys. Chem. Chem. Phys. 10 (2008) 3561.
[9] O.A. Oviedo, M.M. Mariscal and E.P.M. Leiva. Phys. Chem. Chem. Phys. 12 (2010) 4580.
[10] G. Ouyang, C. X. Wang, and G. W. Yang. Chem. Rev. 109, 4221, (2009).
[11] Underpotential deposition, From Fundaments and Theory to Applications at the Nanoscale". O. A. Oviedo, L. Reinaudi, S. García y E. P. M. Leiva. "Monographs in Electrochemistry". Springer. (2016).
[12] Metal Clusters and Nanoalloys: From Modeling to Applications". Serie "Nanostructure Science and Technology". Edited by M. M. Mariscal, O. A. Oviedo and E. P. M. Leiva. Editorial Springer. (2013).

View Article Online
DOI: 10.1039/C6CP05718G

[13] Modelling of Metal Electrodeposition at the Nanoscale", O. A. Oviedo and E. P. M. Leiva. Handbook of Nanoelectrochemistry: Electrochemical Synthesis Methods, Properties and Characterization Techniques. Editorial Springer. Editado por Z.A. Niknam. (2015).
[14]N. Tian, Z-Y Zhou, S-G. Sun, Y. Ding, Z. L. Wang. Science 316 (2004) 732
[15] M. L. Personick, M. R. Langille, J. Zhang, C. A. Mirkin. Nano Lett. 11 (2011) 3394
[16] M. R. Langille, M. L. Personick, J. Zhang, and C. A. Mirkin. J. Am. Chem. Soc. 134 (2012) 14542
[17] N. Tian, Z-Y. Zhou, and S-G. Sun. J. Phys. Chem. C 112 (2008) 19801
[18] Z-Y. Zhou, N. Tian, Z-Z. Huang, D-J. Chen and S-G. Sun. Faraday Discuss. 140 (2008) 81
[19] J. W. Hong, M. Kim, Y. Kim, and S. W. Han. Chem. Eur. J. 18 (2012) 16626
[20] D. Astruc, Nanoparticles and Catalysis. Wiley VCH (2008)
[21] N Tian, Z-Y. Zhou, N-F. Yu, L-Y. Wang, and S-G Sun. J. Am. Chem. Soc. 132 (2010) 7580
[22] D.M. Kolb and F.C. Simeone, Electrochim. Acta 50,2989, (2005)
[23] N. B. Luque, L. Reinaudi, P. Serra, E. P.M. Leiva. Electrochim. Acta 54 3011, (2009)
[24] Luque, N.B., Del Pópolo, M.G., Leiva, E.P.M. Anales de la Asociación Química Argentina 91 (2003) 65-72
[25] Luque, N.B., Leiva, E.P.M. Electrochimica Acta 50 (2005) 3161-3178
[26] Luque, N.B., Del Pópolo, M.G., Leiva, E.P.M. Surface Science 571 (2004) L319-L324
[27] Del Pópolo, M.G., Leiva, E.P.M., Mariscal, M., Schmickler, W. Surface Science 597 (2005) 133-155
[28] Mariscal, M., Narambuena, C.F., Del Pópolo, M.G., Leiva, E.P.M. Nanotechnology 16 (2005) 974-980
[29] W. Li, G.S. Hsiao, D. Harris, R:M. Nyffenegger, J.A. Virtanen, R.M. Penner, J. Phys. Chem. 100 (1996) 20103.
[30] X.H. Xia, R. Schuster, V. Kirchner, G. Ertl. J. Electroanal. Chem. 461 (1999) 102.
[31] D. Hofmann, W. Schindler, J. Kirchner. Appl. Phys. Lett. 73 (1998) 3279.
[32] M.M. Mariscal, E.P.M. Leiva, S.A. Dassie. J. of Electroanalytical Chemistry 607 (2007) 10.
[33] T. Solomun and W. Kautek. Electrochim. Acta 47 (2001) 679.
[34] M.M. Mariscal, E.P.M. Leiva. "Computer Simulations of Electrochemical Low-Dimensional Metal Phase Formation", in Electrocrystallization in Nanotechnology Edited by G. Staikov. John Wiley & Sons, Inc. (2007).
[35] E.P.M. Leiva. "Nanoelectrochemistry" in Fundamentals of Electrochemistry, Second Edition, Edited By V. S. Bagotsky. John Wiley & Sons, Inc. 2006
[36] O.A. Pinto, B.A. Lopez de Mishima, E.P.M. Leiva, O.A. Oviedo. Physical Review E 86 (2012) 061602.
[37] O.A. Pinto, B.A. Lopez de Mishima, M. Dávila, A.J. Ramirez Pastor, E.P.M. Leiva and O.A. Oviedo. Phys. Rev. E, 88 (2013) 062407.
[38] Pinto, O. A., de Mishima, B. L., Leiva, E. P. M., and Oviedo, O. A. Physical Chemistry Chemical Physics, 18(21) (2016) 14610-14618.
[39] M.E.J. Newman and G.T. Barkema, Monte Carlo Method in statistical physics, Clarenton –Press Oxford, (1999).

[40] H. B. Callen, "Thermodynamics and an introduction to thermostatistics", John Wiley and Sons, (1985).
[41] D. Nicholson, N.G. Parsonage, "Computer Simulation and the Statistical Mechanics of Adsorption", Academic Press, London, (1982).
[42] N. Metropolis, A. W. Rosenbluth, M. N. Rosenbluth, A. H. Tellery and E. Teller. J Chem Phys. 21 (1953) 1087.
[43] E. Budevski, G. Staikov, W. J. Lorenz, "Electrochemical Phase Formation and Growth: An Introduction to the Initial Stages of Metal Deposition". VCH Verlagsgesellschaft mbH (1996).